Neurobiology of Disease 146 (2020) 105079

Contents lists available at ScienceDirect

Neurobiology of Disease

journal homepage: www.elsevier.com/locate/ynbdi

Fibrillation and molecular characteristics are coherent with clinical and pathological features of 4-repeat tauopathy caused by MAPT variant G273R

Alexander Sandberg[a,1], Helen Ling[b,1], Marla Gearing[c,d], Beth Dombroski[e], Laura Cantwell[e], Lea R'Bibo[f], Allan Levey[d], Gerard D. Schellenberg[e,g], John Hardy[h,i], Nicholas Wood[f], Josefin Fernius[a], Sofie Nyström[a], Samuel Svensson[a,j], Stefan Thor[k], Per Hammarström[a,*], Tamas Revesz[b,**], Kin Y. Mok[h,l,***]

[a] Department of Physics Chemistry and Biology, Linköping University, Linköping, Sweden
[b] Queen Square Brain Bank for Neurological Disorders, Queen Square Institute of Neurology, University College London, London, UK
[c] Department of Pathology and Laboratory Medicine, Goizueta Alzheimer's Disease Research Center, Emory University School of Medicine, Atlanta, GA, USA
[d] Department of Neurology and Goizueta Alzheimer's Disease Research Center, Emory University School of Medicine, Atlanta, GA, USA
[e] Department of Pathology and Laboratory Medicine, Perelman School of Medicine, University of Pennsylvania, Philadelphia, PA, USA
[f] Department of Clinical and Movement Neurosciences, UCL Institute of Neurology, University College London, London, UK
[g] Department of Genetics, Perelman School of Medicine, University of Pennsylvania, Philadelphia, PA, USA.
[h] UK Dementia Research Institute at UCL and Department of Neurodegenerative Disease, UCL Institute of Neurology, University College London, London, UK
[i] Institute for Advanced Study, The Hong Kong University of Science and Technology, Hong Kong, SAR, China
[j] CBD Solutions, Stockholm, Sweden
[k] School of Biomedical Sciences, The University of Queensland, Brisbane, Qld 4072, Australia
[l] Division of Life Science, The Hong Kong University of Science and Technology, Hong Kong, SAR, China

ARTICLE INFO

Keywords:
MAPT
G273R
Pathology
4-repeat tau
Tauopathy
Corticobasal degeneration
CBD
Progressive supranuclear palsy
PSP
Aggregation propensity

ABSTRACT

Microtubule Associated Protein Tau (MAPT) forms proteopathic aggregates in several diseases. The G273R tau mutation, located in the first repeat region, was found by exome sequencing in a patient who presented with dementia and parkinsonism. We herein return to pathological examination which demonstrated tau immunoreactivity in neurons and glia consistent of mixed progressive supranuclear palsy (PSP) and corticobasal degeneration (CBD) features. To rationalize the pathological findings, we used molecular biophysics to characterize the mutation in more detail *in vitro* and in *Drosophila*. The G273R mutation increases the aggregation propensity of 4-repeat (4R) tau and alters the tau binding affinity towards microtubules (MTs) and F-actin. Tau aggregates in PSP and CBD are predominantly 4R tau. Our data suggest that the G273R mutation induces a shift in pool of 4R tau by lower F-actin affinity, alters the conformation of MT bound 4R tau, while increasing chaperoning of 3R tau by binding stronger to F-actin. The mutation augmented fibrillation of 4R tau initiation *in vitro* and in glial cells in *Drosophila* and showed preferential seeding of 4R tau *in vitro* suggestively causing a late onset 4R tauopathy reminiscent of PSP and CBD.

1. Introduction

Microtubule-associated protein tau (MAPT), encoded by *MAPT* gene, is important for the formation and maintenance of microtubules (Weingarten et al., 1975). Point mutations of the *MAPT* gene and the associated expressed tau protein plays a central role in multiple neurodegenerative diseases, including Alzheimer's disease (AD), Frontotemporal lobar degeneration (FTLD), Progressive supranuclear palsy

* Correspondence to: Professor Per Hammarström, Department of Physics Chemistry and Biology B-Huset, Linköping University, Entrance 21, Room 2B.680, Campus Valla, Linköping SE-581 83, Sweden.
** Correspondence to: Professor Tamas Revesz, Queen Square Brain Bank for Neurological Disorders, UCL Queen Square Institute of Neurology, 1 Wakefield Street, London WC1N 1PJ, UK.
*** Correspondence to: Dr Kin Y MOK, UK Dementia Research Institute at UCL and UCL Queen Square ION Department of Neurodegenerative Disease, Wing 1.2 Cruciform Building, Gower Street, London WC1E 6AU, UK.
E-mail addresses: per.hammarstrom@liu.se (P. Hammarström), t.revesz@ucl.ac.uk (T. Revesz), k.mok@ucl.ac.uk (K.Y. Mok).
[1] *These are co-first authors and contributed equally to the study.*

https://doi.org/10.1016/j.nbd.2020.105079
Received 3 November 2019; Received in revised form 2 September 2020; Accepted 5 September 2020
Available online 19 September 2020

(PSP), and corticobasal degeneration (CBD). Currently, 108 familial mutations are documented in the Alzforum Alzgene Database (Alzforum, 2019; Rosler et al., 2019). Not only do different mutations of MAPT gene lead to different clinical phenotypes and neuropathological features, heterogeneity is not uncommon within the same mutation, for instance, various clinical phenotypes and abnormal tau accumulation were reported in *MAPT* A152T (Kara et al., 2012). On the other hand, clinical presentation of frontotemporal dementia is associated with different genetic mutations (Database, A.F.M, 2019; Greaves and Rohrer, 2019).

Such heterogeneity also extends to the clinicopathological aspect. Pathologically confirmed PSP and CBD may have more than one clinical presentation (Williams et al., 2005). On the other hand the classic Richardson's syndrome and corticobasal syndrome are not always caused by respectively underlying PSP and CBD pathologies (Ling et al., 2010).

As part of a large-scaled study on the genetics and pathology of CBD, we identified 361 cases with a diagnostic label of CBD across brain banks in Europe, North America and Australia. Exome sequencing was performed for the genetic arm of the study. A rare *MAPT* mutation was identified in one case in the exome sequenced cohort translating to a G273R mutation of the tau protein. In this study, we report the clinical and pathological features of this case and investigated the potential role of this rare mutation in tauopathy.

It is a conundrum why certain tauopathies show predominantly 3R (Picks disease), 4R (PSP and CBD) or mixed 3R + 4R (Alzheimer's disease) tau aggregates. We hence complemented the pathological studies with molecular biophysics and transgenic *Drosophila* experiments using 3R and 4R tau variants to study the effect of the mutation in these two different tau isoform models enabling us to rationalize why a predominantly 4R pathology could be caused by the G273R mutation.

2. Methods

DNA were extracted from the frozen brain or obtained from the storage of the respective brain banks. All DNA were sent to University of Pennsylvania GS's laboratory. Whole exome sequence were done using Agilent SureSelect Capture v5 (Santa Clara, CA, USA), and was sequenced with Illumina HiSeq (San Diego, CA, USA).

Variant calling: The fastq file of sequencing reads was mapped to Human b37 reference genome using Novoalign v3 (Novocraft technologies, Selangor, Malaysia) with default parameters. The aligned sequences were saved in BAM files. The files were then processed according to the GATK Best practices (https://gatkforums.broadinstitute.org/gatk/) and is summarized as follow: For each individual Exome data, duplicates was marked with PICARD (v1.114) (http://picard.sourceforge.net/), recalibrated with Base Quality Score Recalibration using GATK v3.7, and variant called with GATK HaplotypeCaller v3.7. The cohort gvcf files were combined using GATK CombineGVCFs and group variant joint called with GATK GenotypeGVCFs. The cohort's variant was filtered as suggested (Carson et al., 2014): Initially with hard genotype filters and variant filter genotype, then followed by GATK variant quality score recalibration (VQSR). Annotation of the variants called was done with Annovar (Wang et al., 2010). The variant identified was confirmed by Sanger sequencing. (Primer and protocol in supporting information 1 & Fig. S1).

2.1. Pathology

Unstained tissue slides of the anterior frontal cortex, temporal cortex, parietal cortex, hippocampus, striatum and midbrain were obtained for pathological review from Emory University. Hematoxylin and eosin stain and immunohistochemistry using tau (AT8 clone; Thermo scientific MN1020; 1:600) and amyloid-β peptide (Biosource international, Camarillo, CA, Mouse Dako, clone 6F/3D; 1:100) antibodies were performed in all available tissue sections. Additional staining including Gallyas silver stain, alpha-B crystallin and 3-repeat and 4-repeat tau immunohistochemistry were unfortunately not possible due to limited tissue availability for this historical case.

2.2. Transgenic Drosophila

Tissue specific expression was achieved by using transgenic *Drosophila melanogaster* and the GAL4/UAS system. The driver lines used was *n-syb-Gal4* (neuronal expression) (Jonson et al., 2015), and *repo-Gal4* (glial expression) (Sepp et al., 2001). UAS lines were *UAS-Tau 0N3R and UAS-Tau 0N4R (*Fernius et al., *2017)*; *UAS-Tau 0N3R G273R*, and *UAS-Tau 0N4R G273R (this study)*, *UAS-Aβ 1–42* (Jonson et al., 2015) and control (*OregonR*). The sequence coding for human Tau was codon optimized for expression in *Drosophila* (www.kazusa.or.jp/codon/cgi-bin/showcodon.cgi?species). Sequences were added to the 5′: a consensus start codon (Cavener and Ray, 1991) and an *Eco*RI site, as well as to the 3′; three different stop codons (amb, och, opa) and an *Xba*I site (see Suppl. Info. 2 for all sequences). DNAs were generated by gene-synthesis (Genscript, New Jersey, USA), and cloned into pUASattB (Bischof et al., 2007), as EcoRI/XbaI fragments. DNAs were injected into landing site strain BL#9736 (53B) (BestGene, CA, USA).

Stocks were maintained at 25 °C under 12:12 h light:dark cycles. Stocks and crosses were reared in 50 ml vials containing standard *Drosophila* food (containing water, agar, molasses, cornmeal, yeast, nipagin, ethanol and propionic acid).

2.3. Tau protein concentration determination of Drosophila

5 day old *UAS-Tau* flies crossed with *n-syb-Gal4* and *repo-Gal4* were harvested and frozen at −80 °C, and stored there until further use. During preparation, all samples where kept on ice and centrifugation was done at 4 °C, unless stated otherwise. Frozen flies were decapitated and heads from 20 males and 20 females from each crossing was homogenized 2 min in pre-cold Tris buffer (25 mM tris, 15 mM NaCl, 1 mM EDTA, 1 mM EGTA, pH 7.4). Samples were centrifuged for 3 min at 3000 *g* to remove debris of exoskeleton and the homogenate solution was further used. The homogenate was centrifuged at 100,000 *g* in a Beckman ultracentrifuge for 1 h. Samples from the ultracentrifugation were split into “supernatant” and “pellet”. All samples where diluted with GuHCl to a final concentration of 4.67 M GuHCl and equal volumes. The samples where incubated over night at room temperature under vigorous shaking. For concentration determination of tau the samples were diluted to a final concentration of 0.1 M GuHCl. Tau concentration determination was done using a Mesoscale discovery (MSD) multispot total tau assay kit with appended concentration reference and performed according to the manufacturer's recommendations.

2.4. Tau aggregate relative quantification in Drosophila brain

5 day old flies from all *UAS-tau* variants crossed with *n-syb-Gal4* and *repo-Gal4* were sedated in CO_2, decapitated and embedded in cryosection OCT media, frozen and stored at −80 °C until further use. Sections were made to 10 μm fixed in 70% cold ethanol, hydrated, blocked and incubated with 1 μM p-FTAA for 30 min as described previously (Jonson et al., 2015; Berg et al., 2010; Nilsson et al., 2018). Sections were washed and mounted with Dako fluorescence mounting medium and imaged in a Leica DM6000 epifluorescence microscope equipped with a spectral cube hyperspectral imaging camera (ASI). Fluorescence images were collected using 436 nm excitation and emission intensities at 540 nm were selected.

2.5. Expression, purification and characterization of recombinant tau

Expression and purification of recombinant tau for *in vitro* experiments was performed as described previously (Jonson et al., 2015). In short, the 0N4R PWT sequence cloned in a pNIC vector and the other

three sequences were inserted in pET-21A(+) vectors. In all variants the two endogenous cysteines have been replaced by serines (C291S and C322S) rendering a pseudo-wild type (PWT) sequence to prevent disulfide bond formation without adding reducing agent and allowing for a chemically stable environment during long time periods. Plasmids containing the 0N4R PWT, 0N4R G273R PWT, 0N3R PWT and 0N3R G273R PWT were transformed into *E. coli* BL21/DE3 cell and cultures were grown to a OD of 0.6. Protein expression was induced using 0.5 mM IPTG (Isopropyl-β-D-thiogalactopyranoside (UPBbio)) and thereafter incubated for 4 h. Cells where harvested by centrifugation for 30 min at 4000 *g*, the pellet was dissolved in dH_2O, frozen in liquid nitrogen and stored at −80 °C until needed.

Harvested cells were thawed and centrifuged at 16,000 *g* for 10 min at 4 °C. The pellet was dissolved in equilibration buffer (EQ-buffer) (50 mM Tris HCl (MP Biomedicals, LLC), 300 mM NaCl and 30 mM Imidazol (AppliChem) pH 7.4) sonicated 2 min at 30% of maximum amplitude (Bransson Digital sonifier), followed by boiling for 20 min followed by centrifugation for 10 min at 16,000 g. The supernatant was applied to a HisTrap FF crude column (GE Healthcare) equilibrated with EQ-Buffer, washed with 5 column volumes EQ-Buffer and eluted with 150 mM imidazole in EQ-buffer. Fractions containing Tau were dialyzed against dH_2O followed by lyophilization. Lyophilized pellets were stored in −80 °C until needed. Lyophilized pellets were dissolved in 6 M guanidine HCl (MP Biomedicals) incubated overnight and subjected to size exclusion chromatography on a Sephacryl S200 column pre-equilibrated in running buffer (PBS-Tablets 140 mM NaCl, 2.7 mM KCl, 10 mM Phosphate, pH 7.4 from Medicago with 0.02% *w/v* of sodium azide). Fractions containing monomeric non-truncated Tau was used in all the assays determined by coomassie stained SDS-PAGE.

2.6. Fibrillation assays

Recombinant tau was added to PBS buffer in a Corning 96-well half area non treated black with clear flat bottom plate (Costar 3880) to a final concentration of 6 μM with 60 μg/ml Heparin and 0.3 μM p-FTAA, a fluorescent amyloid ligand (Sandberg and Nystrom, 2018; Aslund et al., 2009). All experiments were run in triplicates. Preformed fibrils from previous aggregation reactions performed under the same conditions were used as seeds (10% *v/v*). The fibrillation plate was incubated in a Tecan infinite M 1000 instrument at 37 °C, 60 s shaking (amplitude 2 mm, 654 rpm) and emission intensity (λ_{ex} 440 nm, λ_{ex} 480–650 nm) measured every 30th minute. The lag time was defined as the time needed for emission at 510 nm to reach half of maximum intensity ($T_{1/2}$) (Gade Malmos et al., 2017). Average $T_{1/2}$ and standard deviations were calculated and unpaired *t*-test with Welch's correlation was performed using GraphPad prism 8.0.1.

2.7. Binding affinity to Heparin by isothermal calorimetry (ITC)

Heparin and tau were dialyzed against the same PBS buffer using a 3kD cutoff dialysis membrane (Spectrapor) and measurements were done in a Microcal PEAQ-ITC instrument from Malvern. The ITC cell was loaded with 50 μM Tau and 1 mM Heparin (H5515-100KU, Heparin Sodium Salt from porcine intestinal mucosa, Sigma-Aldrich) was injected. The instrument settings were: 25 °C; reference power: 4 μcal/s; feedback: high; stir speed: 750 rpm; initial delay: 60 s; number of injections: 36; first injection: 0.4 μl and the following injections 1 μl. Results were evaluated using the Microcal PEAQ-ITC analysis software. Average and standard deviations were calculated and an unpaired *t*-test was done using GraphPad prism 8.0.1.

2.8. Microtubule (MT) and F-actin binding assays

For the binding assays, MULTI-ARRAY 96-well plates (L15XA-3, Meso Scale Discovery. MD, USA) were used. All samples run in triplicates. All steps except step 5 included incubation for 1 h under agitation (planar shaking at 500 rpm) in room temperature followed by a 3 × 5 min wash with 150 μl 1 X washing buffer (R61TX-2, Meso Scale Discovery. MD, USA).

1. The plate was coated with 25 μl F-actin 0.2 mg/ml or taxol-stabilized microtubuli 0.1 mg/ml (Cat. AD99-B and MT002-XL from Cytoskeleton, Inc. Denver, CO, USA), incubated and washed.
2. Blocking was performed with 25 μl 3% Blocker A (R93BA-1, Meso Scale Discovery. MD, USA).
3. 25 μl monomeric recombinant tau was added, incubated and washed.
4. 25 μl of both primary (Anti-Tau-1, clone PC1C6, Merck Millipore) and secondary antibody (R32AC-5, MSD Sulfo-Tag Goat Anti mouse) was added 3 μg/ml of each, incubated and washed.
5. Read buffer (R92TC-2, Meso Scale Discovery. MD, USA) was added and plates were read within 15 min using a SECTOR Imager 2400 instrument (Meso Scale Discovery. MD, USA).

Standard curves were generated using free monomeric tau bound directly to the MULTI-ARRAY 96-well plates. Concentrations were calculated using the MSD software. Log EC_{50} values were calculated and comparative Log EC_{50} fits were made using weighted least squares regression in GraphPad prism 8.0.1.

2.9. Transmission electron microscopy (TEM)

5 μl aliquots of tau fibril samples were added to a carbon coated cupper grids (Ted Pella Inc.) and were incubated for 60 s. Sample was washed with dH_2O, incubated with 2% uranyl acetate solution for 30 s and blotted dry. Images were acquired in a Jeol 1230 electron microscope operating at 100 kV using a Gatan digital camera. Widths of fibrils (n = 84) was measured manually using imageJ. Averages and standard deviations were calculated and an unpaired *t*-test with Welch's correlation was used was performed using GraphPad prism 8.0.1. The corresponding TEM preparation and imaging procedure was used for imaging F-actin and taxol stabilized MT.

3. Results

Of the 361 exomes that were sequenced, the mean coverage is ~69× with ~98.7% covering at least 6×, & 96.0% about 15× and a rare non-synonymous mutation in *MAPT* was identified (hg19 chr17:44,074,025; NM_005910:exon8:c.G817A:p.G273R) in a single patient with H1H1 haplotype. The mutation was confirmed by Sanger sequencing (Fig. S2). We found only one additional non-synonymous variant in the exons of *MAPT*, rs2258689, in this case. This variant occurs in ~27.5% of population in ExAC. No splice site or frame shift mutations were found. (Further details in the supplementary Table 1).

3.1. Clinical summary

The subject was a right-handed white male retired air force pilot with 14 years of education, and a past history of hypertension and alcohol abuse. He was evaluated clinically at the Department of Neurology at Emory University by both cognitive and movement disorders specialists as well as neuropsychology, and he participated in an observational study with annual research evaluations at the Emory Alzheimer's Disease Research Center. He was first evaluated at the age of 74 with a history of 3 years of progressive memory decline and tremor. Initial symptoms included forgetting recent events and conversations, losing his personal belongings, and getting lost when driving to previously familiar places. He had some episodes of awakening in the middle of the night with confusion. His wife noted that his personality changed with anger over simple incidents and uncharacteristic use of profanity. He had delusions that he was receiving money from the state government. He had developed an asymmetric rest tremor of the left

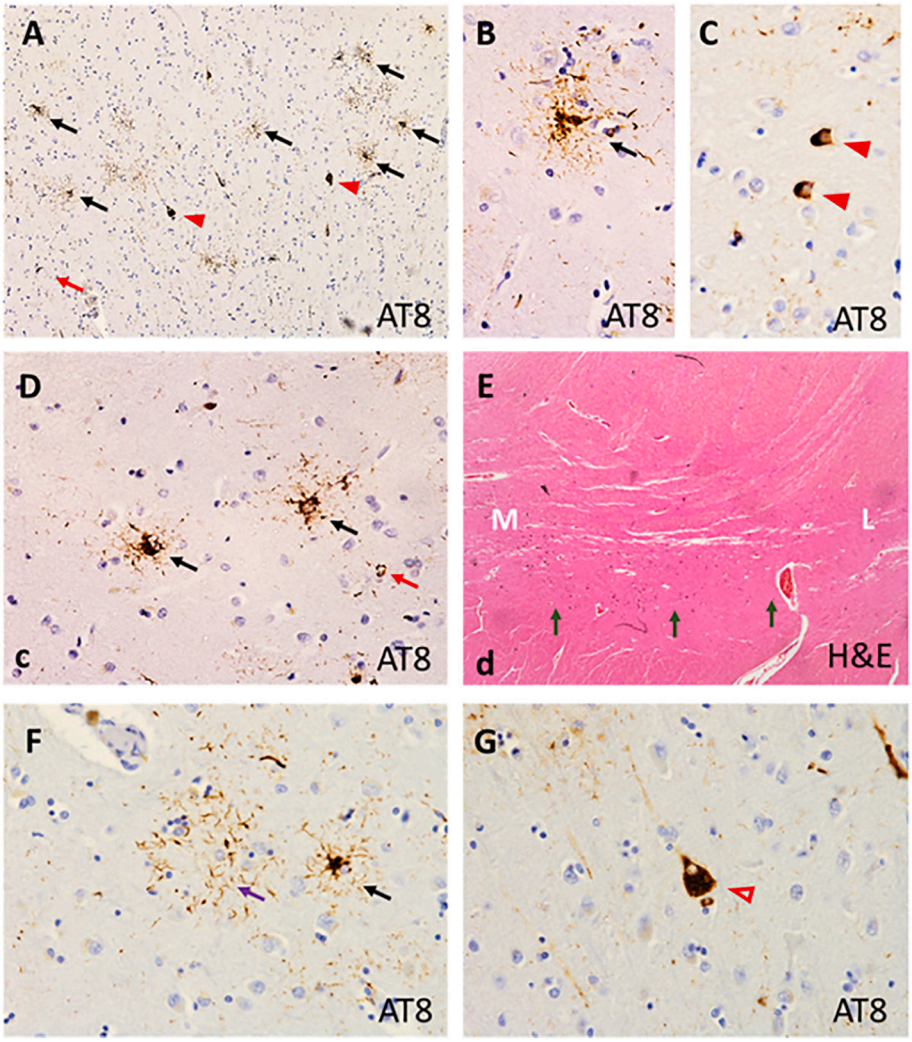

Fig. 1. Tau immunohistochemistry in the anterior frontal cortex shows inclusions in neurons (red arrowheads), astrocytes (black arrows), oligodendroglia (red arrows) and cellular processes (as neuropil threads) in A-D, F, G. Tufted astrocytes (black arrows in B & D), neurofibrillary tangles (red arrowheads in C) and coiled body (red arrow in D) are consistent with the histological features of PSP. In E, severe cell loss predominantly in the lateral substantia nigra (L) with relative preservation in the medial nigra is shown (M). Astrocytic plaque (purple arrow in f) is a pathological hallmark of CBD and does not co-exist with tufted astrocyte (black arrow in f) in sporadic CBD or PSP cases. The presence of swollen neuron (red hollow arrowhead) in the cortices is another characteristic feature of sporadic CBD. The coexistence of PSP and CBD histological features is strongly suggestive of an underlying MAPT mutation. [Objectives: A: x10, B-D, F: x40, E: x2, G: x60]. (For interpretation of the references to colour in this figure legend, the reader is referred to the web version of this article.)

upper extremity about one year after onset of the memory problems. Functionally, he required supervision while performing domestic tasks and in eating, dressing and personal hygiene. His mother had been diagnosed with probable Alzheimer's disease and his sister was reported to have memory impairment (ages of onset undocumented). His initial MMSE score was 24/30, and abnormal findings on general neurological exam included mild cogwheel rigidity and mild rest tremor of the left upper extremity, bradykinetic finger and foot tapping, and snout reflex. Detailed neuropsychological testing revealed moderate to severe deficits involving delayed memory for both verbal and visual material, without sparing of recognition memory, as well as language impairments with dysnomia and poor comprehension. He had difficulty establishing and maintaining a response set and lacked insight regarding his impairments. Visuomotor and visuospatial skills were also below expectation for his estimated premorbid abilities. The clinical diagnostic impression was probable Alzheimer's disease with co-existent Parkinson's disease.

The patient's clinical course continued to progress. Cognitive and motor symptoms worsened annually. He experienced increasing tremor and falls despite partial response to levodopa/carbidopa and a cholinesterase inhibitor. At the last evaluation his Clinical Dementia Rating scale was 2.0, a Dementia Rating Scale of 107/144, with no significant function in home, and requiring much help with personal care as well as incontinence. He died several months after the last evaluation of unknown causes. The final clinical diagnosis of Alzheimer's disease with co-existing Parkinson's disease was reached by a research consensus conference with neurologists and neuropsychologists.

3.2. Neuropathological findings

The weight of the unfixed brain was 1380 g. Macroscopic examination revealed moderate atrophy of the frontal cortex, particularly in a parasagittal distribution, but the remainder of the cortices were unremarkable. Section of midbrain demonstrated a pale substantia nigra with preservation of pigmentation in the most medial regions. No macroscopic brain stem abnormality was identified. At microscopy, there were findings, which were reminiscent of those observed in sporadic progressive supranuclear palsy (Fig. 1a-d). These included frequent tau-immunoreactive neurofibrillary tangles (Fig. 1a-b), tufted astrocytes (Fig. 1b, c), and neuropil threads in the anterior frontal cortex, striatum and substantia nigra. In addition, there were 'atypical' features including sparse atypical astrocytic lesions reminiscent of astrocytic plaques and occasional ballooned neurons with vacuolated cytoplasm in the deep cortical laminae of the superior frontal gyrus. Globose tangles were seen in the substantia nigra. Sparse coiled bodies could be observed in the deep frontal white matter (Fig. 1c). There was severe loss of neuromelanin-containing neurons in the substantia nigra with relative preservation of neurons in the medial nigral subregion. No cell loss was seen in the striatum. There were sparse diffuse and neuritic plaques in the frontal cortex and mild gliosis affecting the superficial regions of the parahippocampal and fusiform gyri. Aβ immunohistochemistry showed sparse mature plaques. There was no evidence of tau-positive grains in the medial temporal lobe structures that were available for histological assessment. The original pathological examination performed at Emory University confirmed the

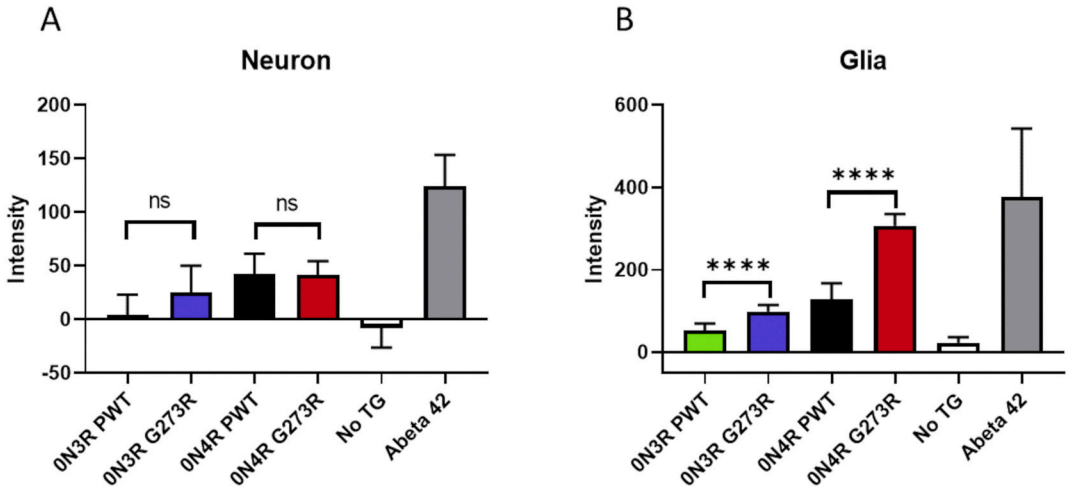

Fig. 2. The amount of aggregates formed in different genotypes of transgenic *Drosophila* expressing 0N3R, 0N4R tau with and without G273R mutation. A positive control expressing Aβ1-42 and a negative control (Oregon-R) were used as references (Jonson et al., 2015). Protein aggregates were quantified as a function of fluorescence intensity of the amyloid specific dye p-FTAA at 540 nm (Berg et al., 2010; Nilsson et al., 2018). Unpaired *t*-test with Welch's correlation was performed * = $P < 0.05$ ** = $P < 0.01$ *** = $P < 0.001$.

absence of Lewy body pathology. In summary, the microscopic findings confirm the diagnosis of a tauopathy with both neuronal and glial accumulation of hyperphosphorylated tau. The mixed astrocytic, tau-positive inclusion profile with both tufted astrocytes and astrocytic plaque-like lesions together with swollen neurons in cerebral neocortex would be supportive of the neuropathological diagnosis of frontotemporal dementia and parkinsonism linked to chromosome 17 due to *MAPT* gene mutation (FTDP-17 *MAPT*).

3.3. Transgenic expression of tau variants in Drosophila

We generated transgenic *Drosophila* that overexpressed 0N4R and 0N3R tau, both wild type and G273R mutants. We used two different Gal4 drivers; neuron specific (*n-syb-Gal4*) and glial cell specific (*repo-Gal4*). To estimate the amount of amyloid fibril aggregates we used the fluorescent probe p-FTAA previously developed by us for amyloid aggregate detection in *Drosophila* (Jonson et al., 2015; Berg et al., 2010; Nilsson et al., 2018). Negative control non-transgenic flies and positive control Aβ1-42 expressing flies were assayed in parallel. In neurons (*n-syb-Gal4*), the amount of aggregates was low and independent of tau genotype (Fig. 2a). In contrast, in glial cells (*repo-Gal4*), we observed an increase of aggregates for the G273R mutant, in both isoforms, when compared to the respective wild type (Fig. 2b). Increased aggregation of G273R hence appeared glia specific in *Drosophila* and was most pronounced for 0N4R G273R.

3.4. Biophysical characterization

The influence of the G273R variant on tau 0N3R and 0N4R fibril formation and interactions with F-actin and MT proteins was investigated using molecular biophysics.

3.5. The seeding activity of Tau is sequence dependent

Fibril formation kinetics were run to assess the effects of the G273R mutation during non-seeded and seeded reactions using different substrates and seeds (Fig. 3 and S4). When performing the fibrillation kinetic experiments heparin was used as a fibrillation inducer. Heparin was necessary to induce fibril formation of tau *in vitro*. Our study is hence a comparative study of WT *versus* G273R mutant to deduce the effect of the point mutation. The 0N4R G273 variant aggregates somewhat faster (T1/2 = 8.3 h) than the corresponding wild type (T1/2 = 10.3 h) (Fig. 3B and C). Preformed fibril seeds were taken from previous kinetic runs performed under the same conditions. Analysis of the seeding activity pattern strongly indicated a sequence similarity pattern. The 0N4R variants are better in seeding 0N4R tau than any of the 0N3R variants regardless of mutation and *vice versa*. The G273R mutant is a better seed for the mutant sequence than the corresponding wild type variant.

3.6. G273R mutant show no significant influence on heparin binding

ITC measurements were performed to investigate if the mutation influenced heparin binding, which in turn might influence the fibrillation kinetics of tau in the *in vitro* fibrillation experiments (Table 1, Fig. S3). The result showed that there were approximately two tau proteins binding to one heparin molecule indicated by a prediction of 0.5 binding sites for all variants. The experiments did not show any significant difference in the dissociation constant (Kd) values between the PWT and G273R mutant for neither 0N3R nor 0N4R Tau (Table 1). These results showed that fibrillation kinetic differences were due to the mutation *per se* and not an effect of differences in affinity for heparin.

3.7. Ultrastructural analysis shows that the G273R mutant affects the fibril morphology

Fibrils were imaged by TEM (Fig. 4). Measurement of fibril width showed that the width varied between mutant and wild type fibrils. The width of 0N3R G273R fibrils (Fig. 4D) was 28.9 ± 8.3 nm and 0N4R G273R fibrils (Fig. 4B) were 22.14 ± 2.9 nm while their corresponding PWT counterparts 0N3R PWT (Fig. 4C) displayed a width of 24.1 ± 6.8 nm and 0N4R PWT (Fig. 3A) 24.55 ± 4.1 nm ($P < 0.001$) respectively. Hence, 0N4R G273R showed thinner fibrils than its corresponding wild type and 0N3R G273R showed thicker fibrils than the wild type (Fig. 4E). The differences in fibril width between the two mutant variants were significant ($P < 0.001$). For the 0N4R PWT and G273R it was evident that there were two different types of fibrils in the sample which were interpreted as straight filaments (SF) and paired helical filaments (PHF) respectively (Fig. 5A-B) (Fitzpatrick et al., 2017). The analysis showed that the both SF and PHF from 0N4R G273R where thinner than SF and PHF from 0N4R PWT (Fig. 5C) emphasizing that the data in Fig. 4E are not due particle imaging bias.

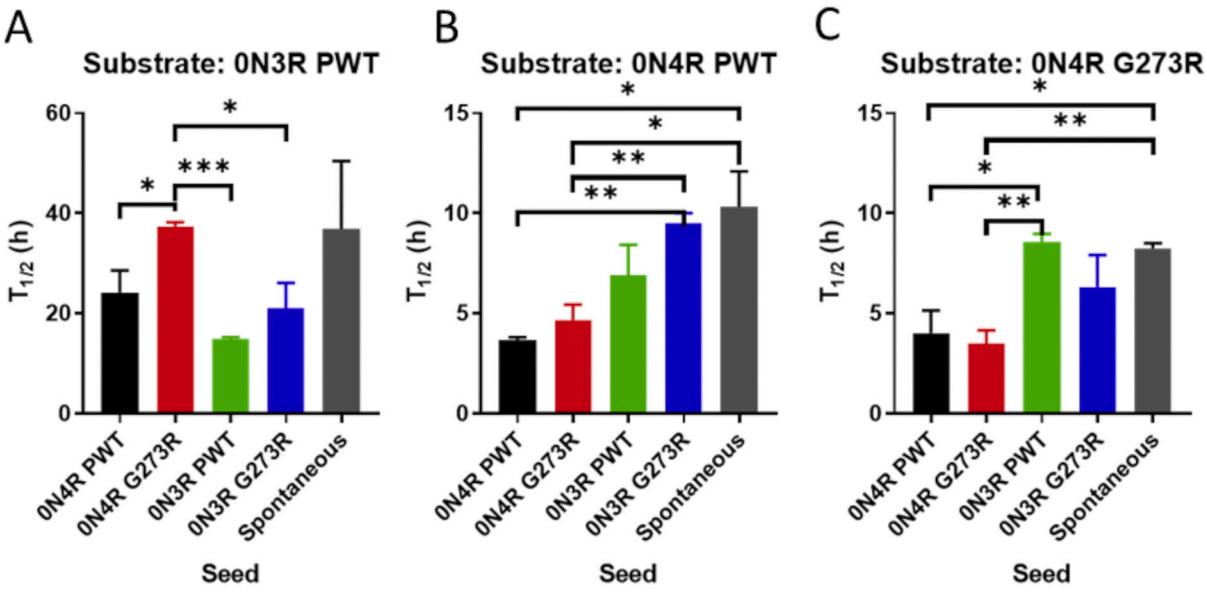

Seed	$T_{1/2}$ (h)
0N4R PWT	24.2 ± 4.4
0N4R G273R	37.4 ± 0.8
0N3R PWT	14.7 ± 0.5
0N3R G273R	21.0 ± 5.1
Spontaneous	36.9 ± 13.5

Seed	$T_{1/2}$ (h)
0N4R PWT	3.7 ± 0.1
0N4R G273R	4.7 ± 0.8
0N3R PWT	6.9 ± 1.5
0N3R G273R	9.5 ± 0.5
Spontaneous	10.3 ± 1.7

Seed	$T_{1/2}$ (h)
0N4R PWT	4.0 ± 1.1
0N4R G273R	3.5 ± 1.1
0N3R PWT	8.6 ± 0.4
0N3R G273R	6.3 ± 1.6
Spontaneous	8.3 ± 0.3

Fig. 3. Graphs showing fibril formation rates expressed as half times of conversion (T1/2) (averages from triplicates and error bars representing standard deviations) from kinetic experiments where 6 μM monomeric Tau (substrate) has been aggregated with 60 μg/ml heparin as inducer and p-FTAA as fluorescent amyloid probe. Spontaneous reaction or reaction seeded with fibrils from previous aggregation experiments are shown. All experiments were run in triplicates. **A**, 0N3R PWT as substrate. **B**, 0N4R PWT as substrate. **C**, 0N4R G273R as substrate. Unpaired t-test with Welch's correlation was performed * = P < 0.05 ** = P < 0.01 *** = P < 0.001. Table to the right show average T 1/2 from triplicates and standard deviation (SD) from the same data as the graphs.

Table 1
Binding affinities of the four different recombinant tau variants used for binding to Heparin, Taxol stabilized microtubules (MT) and F-Actin.

Tau variant	Heparin kD (μM) ± SD	Taxol stabilized microtubule EC 50 (μM) ± Std. Error	F-Actin EC 50 (μM) ± Std. Error
0N4R PWT	3.69 ± 1.48	1.6 ± 0.03	2.7 ± 0.10
0N4R G273R	5.32 ± 1.09	0.9 ± 0.07	6.3 ± 0.21
0N3R PWT	5.35 ± 0.57	2.7 ± 0.14	13.9 ± 0.9
0N3R G273R	5.18 ± 1.5	1.4 ± 0.12	0.7 ± 0.17

3.8. The G273R mutant influences monomeric tau binding to microtubule and F-actin

The tau G273R mutation is located in a MT binding site and close to an F-actin binding site (Cabrales Fontela et al., 2017) (starting at V275 in 4R tau). A binding assay was performed to investigate if binding to these cytoskeletal proteins were affected by the mutation (Cabrales Fontela et al., 2017; Kadavath et al., 2015). The filamentous structure of F-actin and taxol stabilized MTs used for the binding assays were first verified by TEM (Fig. S5A–B). The binding assays for microtubules showed that the 0N4R G273R mutant has a lower EC_{50} value than the 0N4R PWT (Fig. 6A, Table 1), suggesting higher affinity for the mutant. The same trend was observed when comparing 0N3R (Fig. 6B, Table 1). 0N4R PWT bound stronger to microtubules than 0N3R PWT (Fig. 6C, Table 1), the same pattern was observed for the G273R mutant (Fig. 6D, Table 1), consistent with an additional microtubule binding repeat (Cabrales Fontela et al., 2017). When performing the same measurements on F-actin we found that the 0N4R G273R mutant has a higher EC_{50} value than the 0N4R PWT suggesting lower affinity for the mutant (Fig. 7A, Table 1). The opposite effect was found for 0N3R (Fig. 7B, Table 1), where 0N3R wild type showed a poor binding affinity. The variant with the lowest EC_{50} value when binding to F-actin was 0N3R G273R (Fig. 7D, Table 1) suggesting the highest affinity of all tested variants. These data appeared contradictory. We hence speculate that the G273R mutant together with K274 mimics the K280 K281 motif in the F-actin binding site of 0N4R tau by forming an RK *i.e.,* a KK mimic that can form ion bonds with the negatively charged actin. These two pairs may render 0N4R tau ambivalent by intramolecular competition in the 0N4R tau mutant resulting lower affinity for F-actin. For the 0N3R tau G273R mutant *versus* 0N3R wild type, where R2 is missing, the new RK motif in the new context appear to increase F-actin affinity. This reasoning of different binding modes of different tau repeats is compatible with attempts to obtain high resolution structures of tau bound to microtubules, where different synthetic constructs of R1 and R2 repeats bound differently to microtubules (Kellogg et al., 2018). Less is known about tau – actin interactions. To compare the tau variants in a cellular context we quantified the amount of tau in fractionated transgenic *Drosophila* brain homogenates using the fly crossings described above. Tubulin and actin are > 96.4% identical between human and *Drosophila*. Quantification of the amount of expressed tau was rather consistent between all genotypes (Fig. 8a-b). We thereafter analyzed the amount of soluble *versus* pelleted tau in all genotypes by ultracentrifugation (100.000 *g*) of brain homogenates with the expectation that polymerized MT and F-actin would pellet in complex with bound tau. Our results showed higher amounts of tau in the pellet compared to soluble fraction of all genotypes with neuronal expression, with no obvious differences between the genotypes (Fig. 8a). This pattern was consistent, albeit less pronounced in glial cells, for all

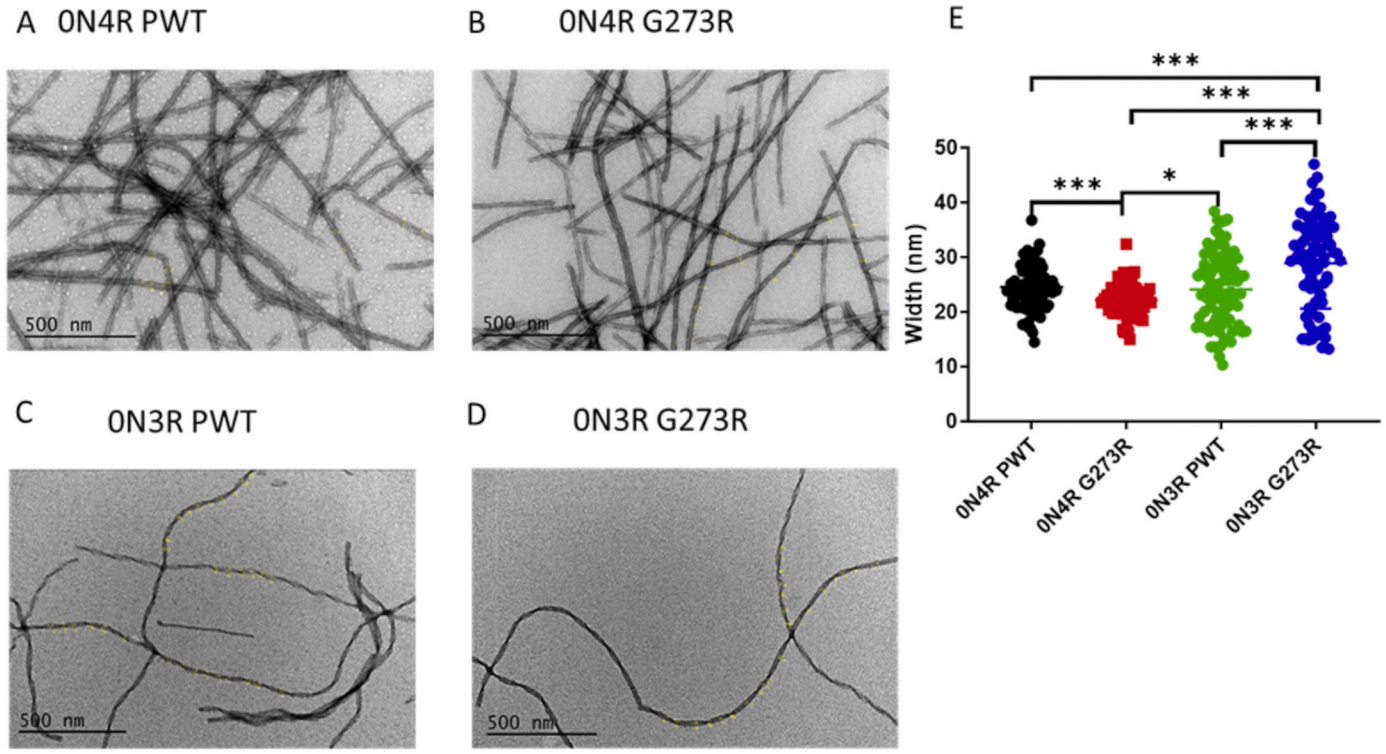

Fig. 4. Left: TEM images of *in vitro* formed tau fibrils, scale bar 500 nm. **A**, 0N4R PWT 24.5 ± 4.1 nm. B, 0N4R G273R 22.1 ± 2.9 nm. C, 0N3R PWT 24.1 ± 6.8 nm. D, 0N3R G273R 28.9 ± 8.3 nm (Averages ± Standard deviations). E, plot of the fibril widths in nm with averages and error bars representing standard deviation. Unpaired t-test with Welch's correlation was used P < 0.05 = *, P < 0.001 = ***.

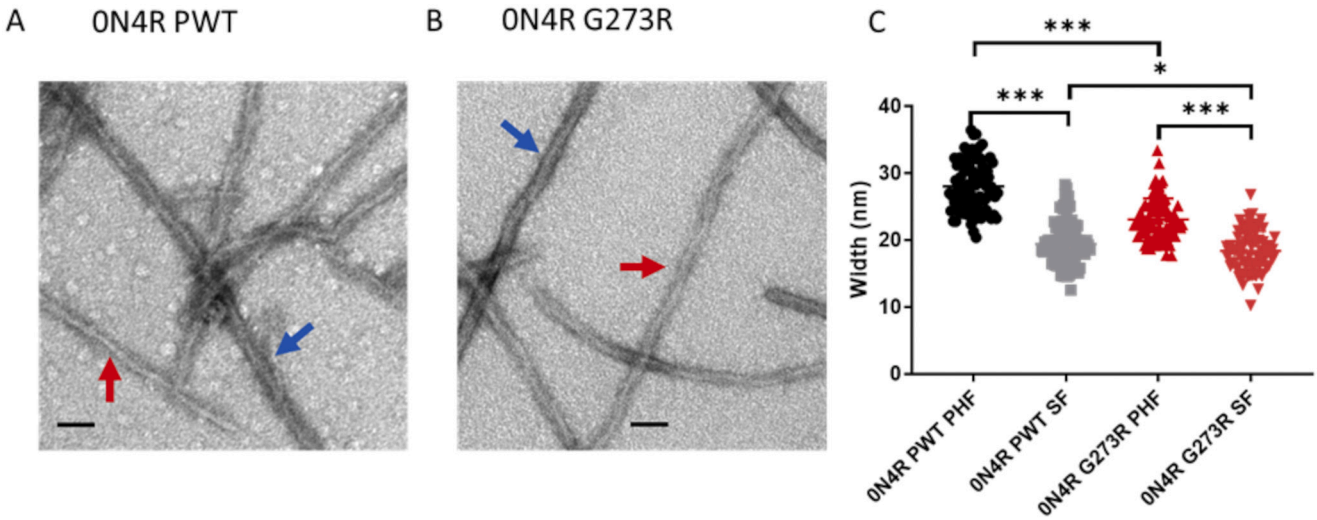

Fig. 5. TEM images of fibrils from A, 0N4R PWT and B, 0N4R G273R. Red arrows indicate presumed straight filaments (SF) and blue arrows indicate presumed paired helical filaments (PHF) scale bar 50 nm. Plot (C) show individual lengths in fibril widths between PWT and mutant and straight filaments to paired helical filaments. Average ± Standard Deviation: 0N4R PWT PHF = 28.0 ± 3.78 nm, 0N4R PWT SF = 19.4 ± 3.50 nm, 0N4R G273R PHF = 23.1 ± 3.14 nm, 0N4R G273R SF = 18.4 ± 2.99 nm. Unpaired t-test with Welch's correlation was used P < 0.05 = *, P < 0.001 = ***. (For interpretation of the references to colour in this figure legend, the reader is referred to the web version of this article.)

genotypes except for 0N3R G273R. For 0N3R G273R the pattern was different and we found higher amounts of tau in the supernatant compared to pelleted tau (Fig. 8b). Interestingly, the 0N3R G273R variant showed the highest affinity for F-actin in the binding assay, suggesting that 0N3R G273R is bound to soluble actin possibly monomeric actin in *Drosophila* glial cells. Hence, the 0N3R G273R variant stands out both with the highest F-actin affinity *in vitro* and in the context of *Drosophila* glial cell sedimentation assay *in vivo*.

4. Discussion

The first report of *MAPT* G273R was made by van der Zee et al. in a case of clinically diagnosed FTLD (van der Zee et al., 2006). The mutation was found in a single case in the cohort. Van der Zee's patient started with memory problems at age 63 and evolved towards FTLD with parkinsonism, based on Neary's criteria (Neary et al., 1998). There were no further details on this mutation.

In our index case, despite limited details, the disease apparently ran

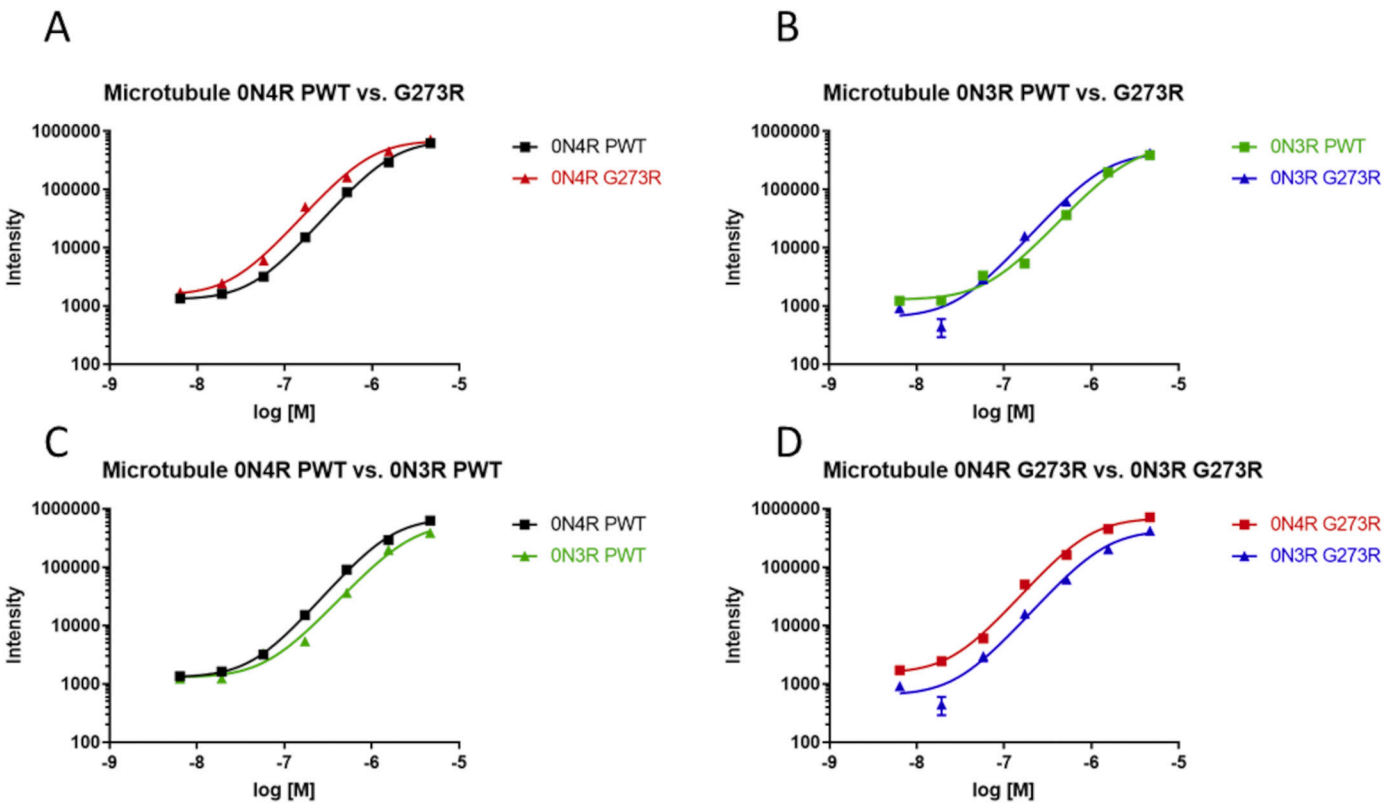

Fig. 6. Carbon surface 96 well plate coated with 0.1 mg/ml Taxol stabilized microtubule for binding of the following tau variants added in different concentrations. A, Show 0N4R PWT and 0N4R G273R for comparison **B**, 0N3R PWT against 0N3R G273R. **C**, 0N4R PWT against 0N3R PWT and **D**, 0N4R G273R against 0N3R G273R. In graphs mean and standard deviation for each concentration. See Table 1 for EC 50 values ± standard error.

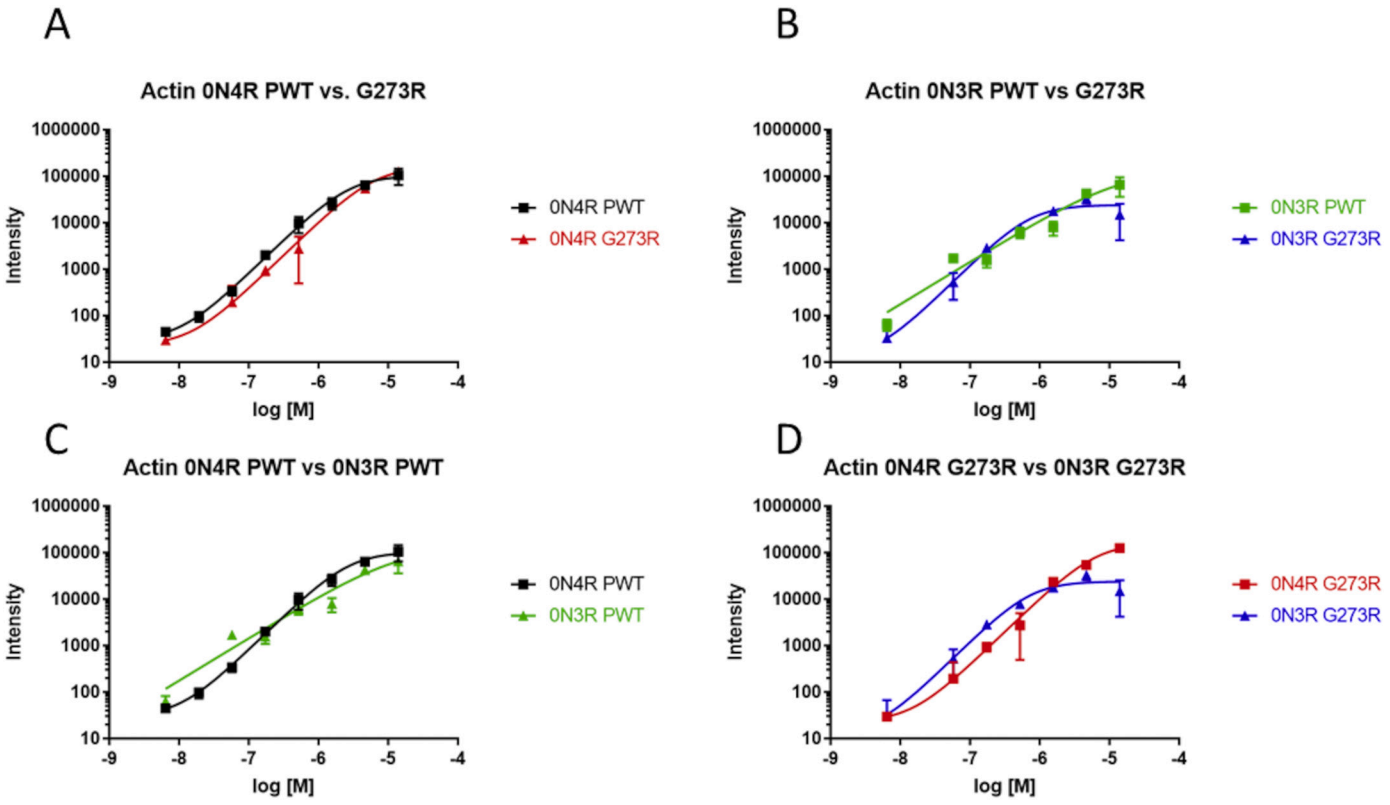

Fig. 7. Carbon surface 96 well plate coated with 0.2 mg/ml F-actin for binding of the tau variants added in different concentrations. **A**, Show 0N4R PWT against 0N4R G273R. **B**, 0N3R PWT against 0N3R G273R. **C**, 0N4R PWT against 0N3R PWT and **D**, 0N4R G273R against 0N3R G273R. See Table 1 for EC_{50} values ± standard error.

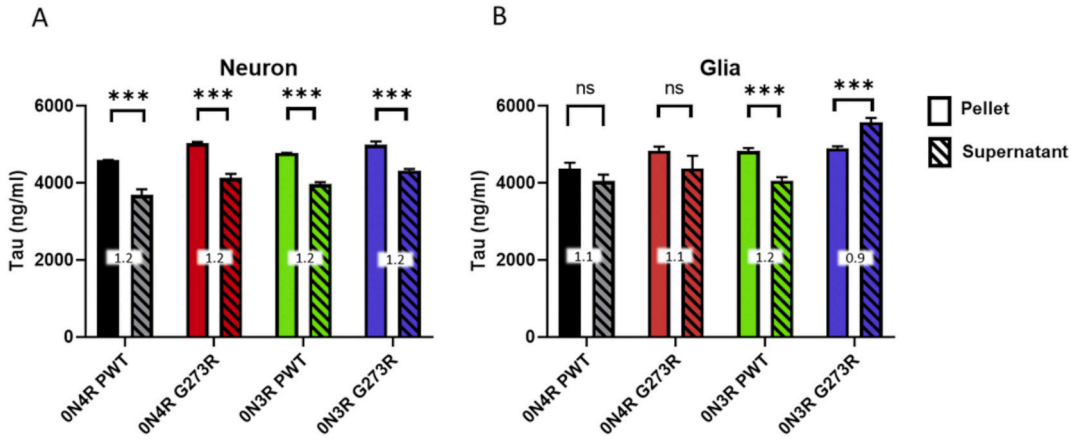

Fig. 8. Quantification of tau of supernatant and pelleted fractions of transgenic *Drosophila* brain homogenates by ultracentrifugation (100.000 *g*). Total amounts were similar between the genotypes. A. Neuronal driver (*n-syb-Gal4*) and B. Glial driver (*repo-Gal4*). The pelleted fraction of tau dominated in all genotypes except for glial expressed 0N3R G273R. The numbers on the graphs display the ratio between pellet and supernatant.

in the family, with the mother and at least one sibling displaying dementia or memory problems. There was no detail about family history in van der Zee's index case. As reported in this patient, *MAPT* mutations are known to cause familial frontotemporal dementia and/or parkinsonian features, hence the term FTDP-17 *MAPT* (Kara et al., 2012). The neuropathological findings of this case include both neuronal and glial accumulation of hyperphosphorylated tau and are most reminiscent of PSP. However, in retrospect, the atypical features, which include ballooned neurons in the superior frontal gyrus and sparse astrocytic plaques would have served as a strong indicator of an underlying *MAPT* gene mutation and CBD pathology (Ling et al., 2016).

4.1. Putative molecular mechanism of the pathogenesis of the G273R tau mutation

Together with the van der Zee (van der Zee et al., 2006) and our study herein now two unrelated patients carrying the *MAPT* G273R were identified to suffer from late onset tauopathy strongly indicating that this is a disease causative tau mutation. The mutation is located in the first highly conserved PGGG repeat involved in microtubulin (MT) binding (Fig. 9A) (Cabrales Fontela et al., 2017). Tauopathies are believed to be caused by tau protein aggregation, leading to toxicity and a loss of neuronal and glial functions. To this end, two questions regarding disease mechanism arise. Firstly, is the mutation more prone to aggregation compared to wild type tau? Secondly, does the mutation alter tau function in stabilizing (binding) cytoskeletal proteins and differently so for 4R *versus* 3R tau? Our fibrillation data suggest a minor but significant increase in the rate of spontaneous fibril formation of 0N4R G273R compared to wild type both *in vitro* and specifically in glial cells of transgenic *Drosophila*. Furthermore, seeding with preformed fibrils preferentially seeded 0N4R G273R mutant tau, while being good as seeding of wild type 0N4R but was inactive in seeding 0N3R wild type. This preferential selectivity in seeding is consistent with a thinner fibril width of 0N4R G273R compared to 0N4R wild type fibrils and especially compared to the 0N3R variants. In summary, this suggests that G273R is a gain-of-toxic function 4R aggregation mutation.

Secondly, our data indicates a modulation of tau binding of cytoskeletal proteins (MT and F-actin) towards stronger binding of MTs for 0N4R tau caused by the G273R mutation while lower affinity for F-actin compared to wild type. While it is beyond the scope of our study to present detailed structural interpretation of our data it is tempting to hypothesize on the effect of the G273R mutation in the context of 3R and 4R tau. Normally, tau binding to MT and F-actin is modulated by addition or removal negatively charged phosphate groups. The G273R mutation increases the positive charge of tau. The increased binding of the 4R G273R mutation to MT is consistent with recent models where low density in Cryo-EM was found for the PGGG repeat by Kellogg and co-workers (Kellogg et al., 2018). Their results showed diffuse binding of full-length tau and only by making synthetic constructs of quadruples of R1 or R2 repeats they obtained a high resolution Cryo-EM density suggesting influence of one repeat over the other. Multiple R2 repeats were shown to bind with higher avidity than multiple R1 repeats towards microtubules consistent with our MT binding data comparing the 3R and 4R variants. Although the PGGG repeat is missing we can based on the Kellogg et al. Cryo-EM structure for R2 (Kellogg et al., 2018), consider a substitution of G to R at the end of R1 right before R2 in the published structure. The new arginine instead of the glycine can likely increase affinity by allowing new electrostatic interactions with acidic residues E420, D427, E431 in β-tubulin as illustrated in Fig. 9B. For tau binding to F-actin less structural information exist in the literature. We found that F-actin binding was highly increased by 0N3R G273R tau compared to wild type 0N3R. This result is interesting, and more studies are needed in order to answer questions regarding the effects of such mutations on the interactions with F-actin and the interplay between the repeat regions of tau as elaborated upon for MT. Furthermore, conspicuously transgenic *Drosophila* with glial expression also suggested altered 3R G273R properties compared to the three other tau variants we studied. Hence, we suggest that altered binding preferences of MT and F-actin of G273R tau in mutant carriers can induce an altered function of monomeric tau either leading to differences in accessible monomer for aggregation or a conformation of MT bound 4R tau being prone to fibril formation. The conformation of 4R G273R tau when bound to MT is likely more rigid than wild type 4R tau and extended towards β-strand structure because of replacement of a flexible glycine with a positively charged arginine residue.

Taken together our molecular biophysics data is consistent with the pathological findings in this patient as CBD and PSP pathology are associated with predominantly 4R tau aggregates. We propose that the G273R mutation induces a shift in pool of 4R tau by lower F-actin affinity, while increasing chaperoning of mutant 3R tau by binding to actin. The G273R mutation shows augmented fibrillation initiation and shows preferential seeding of 4R tau likely leading to a late onset tauopathy.

Acknowledgements

Our work was funded by the Karin & Sten Mortstedt CBD Solutions research grant (Grant code: 512385), Swedish Research Council (2015-04521; 2019-04405), the Göran Gustafsson Foundation, the Swedish

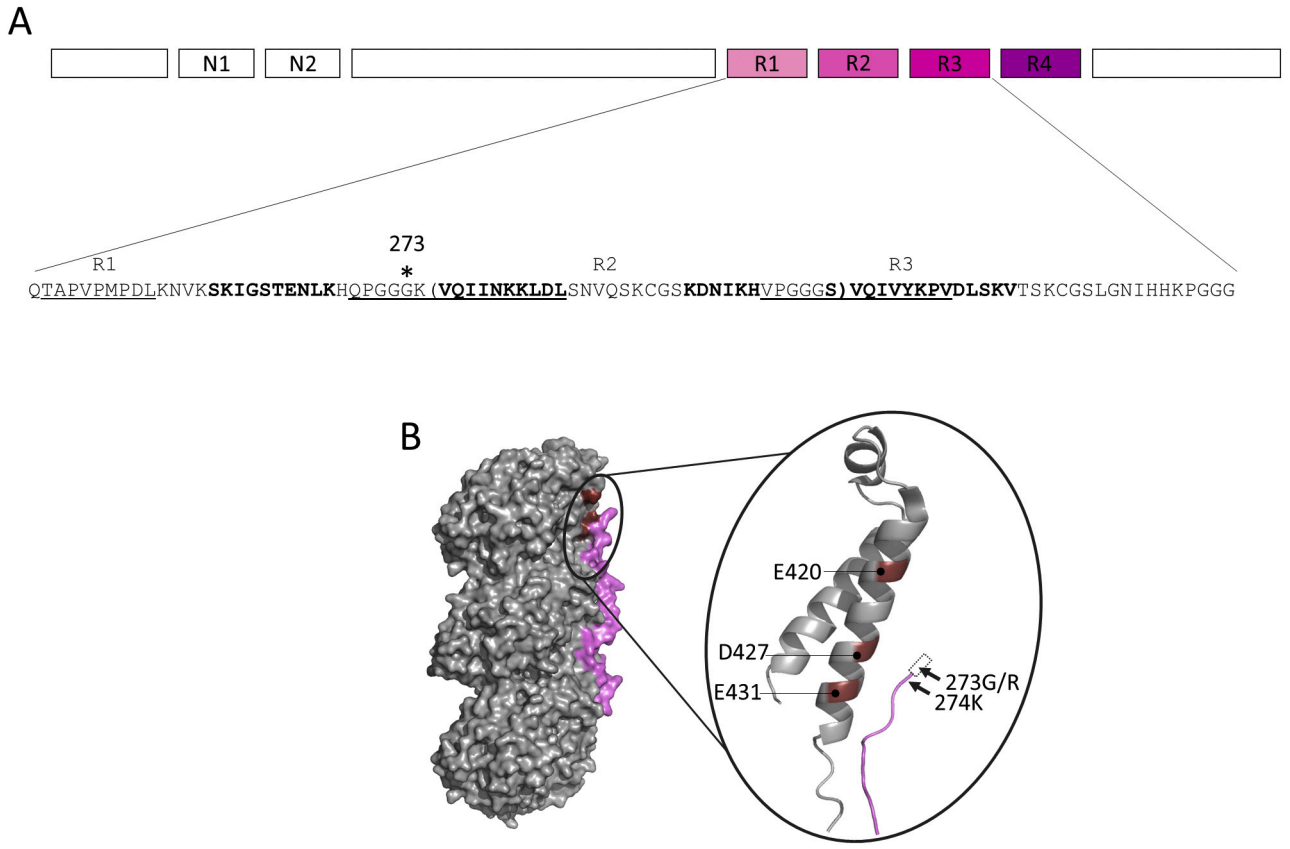

Fig. 9. A, Schematic display of full-length Tau protein with the repeat region colored in magenta. Sequence displayed highlighting the three repeats involved in F-actin and microtubule binding: Underlined = microtubule binding site; Bold = F-Actin binding site; Underline and bold = microtubule and F-actin binding site (according to (Cabrales Fontela et al., 2017)); * = asterisk show the location of G273R mutation; (parenthesis) = Exon 10, Repeat 2 (R2) is excluded in 3R Tau. **B**. Structural illustration, based on the Kellogg et al. structure (Kellogg et al., 2018), of polymerized microtubule as a grey surface with bound R2 tau in magenta. Red surface area highlights tubulin acidic residues E420, D427 and E431. The zoomed in area shows a secondary structure representation of these tubulin acidic residues marked in red on one side of the helix facing tau (magenta) where site 273 would be in close proximity and enable G273R to make electrostatic interactions with MT. (For interpretation of the references to colour in this figure legend, the reader is referred to the web version of this article.)

Alzheimer Foundation, the Swedish Brain foundation, and the Goizueta Alzheimer's Disease Research Center at Emory University (NIH P50 AG025688). We are grateful to Peter Nilsson for providing p-FTAA. We thank Geshanthi Hondhamuni, Kate Strand and Robert Courtney at the Queen Square Brain Bank for their technical support in slide preparation and immunohistochemistry. JH and KYM are currently supported by the UK Dementia Research Institute, which receives its funding from DRI Ltd., funded by the UK Medical Research Council, Alzheimer's Society and Alzheimer's Research UK. JH is supported by Medical Research Council (award number MR/N026004/1); Wellcome Trust (award number 202903/Z/16/Z); Dolby Family Fund; National Institute for Health Research (NIHR) Biomedical Research Centre(BRC) at University College London Hospitals NHS Foundation Trust and University College London. KYM is supported by Michael J Fox Foundation.

Authors' Statement

The study case in this report had given informed consent to participate in the research study.

There is no conflict of interest to report in this case study.

Appendix A. Supplementary data

Supplementary data to this article can be found online at https://doi.org/10.1016/j.nbd.2020.105079.

References

Alzforum. 2019, Alzforum/mutations/mapt. 2019 [cited 2019 July 10]; Available from: https://www.alzforum.org/mutations/mapt.

Aslund, A., et al., 2009. Novel pentameric thiophene derivatives for in vitro and in vivo optical imaging of a plethora of protein aggregates in cerebral amyloidoses. ACS Chem. Biol. 4 (8), 673–684.

Berg, I., Nilsson, K.P., Thor, S., Hammarström, P., 2010. Efficient imaging of amyloid deposits in Drosophila models of human amyloidoses. Nat. Protoc. 5 (5), 935–944. https://doi.org/10.1038/nprot.2010.41.

Bischof, J., et al., 2007. An optimized transgenesis system for Drosophila using germ-line-specific phiC31 integrases. Proc. Natl. Acad. Sci. U. S. A. 104 (9), 3312–3317.

Cabrales Fontela, Y., et al., 2017. Multivalent cross-linking of actin filaments and microtubules through the microtubule-associated protein Tau. Nat. Commun. 8 (1), 1981.

Carson, A.R., et al., 2014. Effective filtering strategies to improve data quality from population-based whole exome sequencing studies. BMC Bioinformatics 15, 125.

Cavener, D.R., Ray, S.C., 1991. Eukaryotic start and stop translation sites. Nucleic Acids Res. 19 (12), 3185–3192.

Database, A.F.M. 2019; Available from: http://www.molgen.ua.ac.be/FTDmutations.

Fernius, J., Starkenberg, A., Pokrzywa, M., Thor, S., 2017. Human TTBK1, TTBK2 and MARK1 kinase toxicity in *Drosophila melanogaster* is exacerbated by co-expression of human Tau. Biol Open 6 (7), 1013–1023. Published 2017 Jul 15. https://doi.org/10.1242/bio.022749.

Fitzpatrick, A.W.P., et al., 2017 Jul 13. Cryo-EM structures of tau filaments from Alzheimer's disease. Nature. 547 (7662), 185–190.

Gade Malmos, K., et al., 2017. ThT 101: a primer on the use of thioflavin T to investigate amyloid formation. Amyloid 24 (1), 1–16.

Greaves, C.V., Rohrer, J.D., 2019. An update on genetic frontotemporal dementia. J. Neurol. 266 (8), 2075–2086.

Jonson, M., et al., 2015. P systematic Aβ analysis in Drosophila reveals high toxicity for the 1-42, 3-42 and 11-42 peptides, and emphasizes N- and C-terminal residues. PLoS One 10 (7), e0133272.

Kadavath, H., et al., 2015. Tau stabilizes microtubules by binding at the interface between tubulin heterodimers. Proc. Natl. Acad. Sci. U. S. A. 112 (24), 7501–7506.

Kara, E., et al., 2012. The MAPT p.A152T variant is a risk factor associated with tauopathies with atypical clinical and neuropathological features. Neurobiol. Aging 33 (9): p. 2231 e7-2231 e14).
Kellogg, E.H., et al., 2018. Near-atomic model of microtubule-tau interactions. Science 360 (6394), 1242–1246.
Ling, H., et al., Does corticobasal degeneration exist? A clinicopathological re-evaluation. Brain, 2010. 133(Pt 7): p. 2045–57.
Ling, H., et al., Astrogliopathy predominates the earliest stage of corticobasal degeneration pathology. Brain, 2016. 139(Pt 12): p. 3237–3252.
Neary, D., et al., 1998. Frontotemporal lobar degeneration: a consensus on clinical diagnostic criteria. Neurology 51 (6), 1546–1554.
Nilsson, K.P.R., Lindgren, M., Hammarström, P., 2018. Luminescent-conjugated Oligothiophene probe applications for fluorescence imaging of pure amyloid fibrils and protein aggregates in tissues. Methods Mol. Biol. 1779, 485–496. https://doi.org/10.1007/978-1-4939-7816-8_30.
Rosler, T.W., et al., 2019. Four-repeat tauopathies. Prog. Neurobiol. 180, 101644.
Sandberg, A., Nystrom, S., 2018. Purification and fibrillation of recombinant human amyloid-beta, prion protein, and tau under native conditions. Methods Mol. Biol. 1779, 147–166.
Sepp, K.J., Schulte, J., Auld, V.J., 2001. Peripheral glia direct axon guidance across the CNS/PNS transition zone. Dev. Biol. 238 (1), 47–63.
van der Zee, J., et al., A Belgian ancestral haplotype harbours a highly prevalent mutation for 17q21-linked tau-negative FTLD. Brain, 2006. 129(Pt 4): p. 841–52.
Wang, K., Li, M., Hakonarson, H., 2010. ANNOVAR: functional annotation of genetic variants from high-throughput sequencing data. Nucleic Acids Res. 38 (16), e164.
Weingarten, M.D., et al., 1975. A protein factor essential for microtubule assembly. Proc. Natl. Acad. Sci. U. S. A. 72 (5), 1858–1862.
Williams, D.R., et al., 2005. Characteristics of two distinct clinical phenotypes in pathologically proven progressive supranuclear palsy: Richardson's syndrome and PSP-parkinsonism. Brain 128, 1247–1258 Pt 6.